Elsevier Editorial System(tm) for Journal of Crystal Growth
Manuscript Draft

Manuscript Number:

Title: Three-dimensional Simulation and Experiment on Micro-floating Zone of LHPG with Asymmetrical Perturbation

Article Type: Special issue: CGCT-5

Section/Category: General subjects

Keywords: A1. Morphological stability
A2. Laser heated pedestal growth
A2. Single crystal growth
B1. Yttrium compounds

Corresponding Author: Professor Peng-Yi Chen, Ph.D

Corresponding Author's Institution: Department of Gemology, Meiho University

First Author: Chia-Yao Lo, Ph.D

Order of Authors: Chia-Yao Lo, Ph.D; Peng-Yi Chen, Ph.D

Abstract: This is a combination of experiments and three-dimensional numerical simulation approach to verify the simulation results of the molten zone shape by experimental data. We study the effect of CO2 laser heating ring and gravity field deviation caused by the space perturbation on micro-floating zone of LHPG during the fiber growth under comparing similar conditions and changing the input parameters of simulation. Our preliminary results compared the molten zone shape are satisfied. The shape of the molten zone (especially the solid-liquid interface) by the asymmetrical heating effect is much larger than the result of gravity field in the simulation results of tilting 3 degrees when the source rod diameter is below 500 microns. And the influence will decrease rapidly with the source rod scale and diameter reduction ratio reducing.These results will help us with the internal flow of the molten zone analysis and developing LHPG crystal fiber growth along horizontal direction in the future.

Dear Editors,

We are pleased to submit our manuscript entitled “Three-dimensional Simulation and Experiment on Micro-floating Zone of LHPG with Asymmetrical Perturbation” by C. Y. Lo, and P. Y. Chen, for possible publication in Journal of Crystal Growth.

In this work, it is a combination of experiments and three-dimensional numerical simulation approach to verify the simulation results of the molten zone shape by experimental data. We study the effect of CO_2 laser heating ring and gravity field deviation caused by the space perturbation on micro-floating zone of LHPG during the fiber growth under comparing similar conditions and changing the input parameters of simulation. Our preliminary results compared the molten zone shape are satisfied. The shape of the molten zone (especially the solid-liquid interface) by the asymmetrical heating effect is much larger than the result of gravity field in the simulation results of tilting 3 degrees when the source rod diameter is below 500 μm. And the influence will decrease rapidly with the source rod scale and diameter reduction ratio reducing.These results will help us with the internal flow of the molten zone analysis and developing LHPG crystal fiber growth along horizontal direction in the future. This manuscript is the authors' original work and has not been published nor has it been submitted simultaneously elsewhere. That all authors have checked the manuscript and have agreed to the submission.

We would be happy to provide additional information if needed.

Sincerely yours

Dr. Peng-Yi Chen

Corresponding Author:

Peng-Yi Chen

Email: x00008415@meiho.edu.tw

Address:

Department of Gemology, Meiho University, Pingtung 91202, Taiwan

Tel.: +886-8-7799821 ext 6506; mobile: +886 -937-388-198

Coauthor:

Chia-Yao Lo, email: cylo@mail.ntou.edu.tw

Tel: +886-2-24622192 ext. 6717

***Highlights**

1. The shape of the molten zone by the asymmetrical heating effect is much larger than the result of gravity field in the simulation results of tilting 3 degrees when the source rod diameter is below 500 μm.
2. The simulation results can be further obtained trend charts of thermal distribution and flow field in molten zone to improve the quality of crystal fiber.
3. The simulation results will help us with the internal flow of the molten zone analysis and developing LHPG crystal fiber growth along horizontal direction in the future.

*Abstract

Three-dimensional Simulation and Experiment on Micro-floating Zone of LHPG with Asymmetrical Perturbation

Chia-Yao Lo[a] and Peng-Yi Chen[b,*]

[a]*Institute of Optoelectronic Sciences, National Taiwan Ocean University, Keelung 20224, Taiwan*

[b]*Department of Gemology, Meiho University, Pingtung 91202, Taiwan*

Abstract

This is a combination of experiments and three-dimensional numerical simulation approach to verify the simulation results of the molten zone shape by experimental data. We study the effect of CO2 laser heating ring and gravity field deviation caused by the space perturbation on micro-floating zone of LHPG during the fiber growth under comparing similar conditions and changing the input parameters of simulation. Our preliminary results compared the molten zone shape are satisfied. The shape of the molten zone (especially the solid-liquid interface) by the asymmetrical heating effect is much larger than the result of gravity field in the simulation results of tilting 3 degrees when the source rod diameter is below 500 μm. And the influence will decrease rapidly with the source rod scale and diameter reduction ratio reducing.These results will help us with the internal flow of the molten zone analysis and developing LHPG crystal fiber growth along horizontal direction in the future.

Keywords: A1. Morphological stability, A2. Laser heated pedestal growth, A2, Single crystal growth, B1. Yttrium compounds

---

Three-dimensional Simulation and Experiment on Micro-floating Zone of LHPG with Asymmetrical Perturbation

Chia-Yao Lo[a] and Peng-Yi Chen[b,*]

[a]*Institute of Optoelectronic Sciences, National Taiwan Ocean University, Keelung 20224, Taiwan*

[b]*Department of Gemology, Meiho University, Pingtung 91202, Taiwan*

Abstract

This is a combination of experiments and three-dimensional numerical simulation approach to verify the simulation results of the molten zone shape by experimental data. We study the effect of CO2 laser heating ring and gravity field deviation caused by the space perturbation on micro-floating zone of LHPG during the fiber growth under comparing similar conditions and changing the input parameters of simulation. Our preliminary results compared the molten zone shape are satisfied. The shape of the molten zone (especially the solid-liquid interface) by the asymmetrical heating effect is much larger than the result of gravity field in the simulation results of tilting 3 degrees when the source rod diameter is below 500 μm. And the influence will decrease rapidly with the source rod scale and diameter reduction ratio reducing.These results will help us with the internal flow of the molten zone analysis and developing LHPG crystal fiber growth along horizontal direction in the future.

Keywords: A1. Morphological stability, A2. Laser heated pedestal growth, A2, Single crystal growth, B1. Yttrium compounds

1. Introduction

Laser-heated pedestal growth method (LHPG) is one of important growth system of producing crystal fiber, which have been shown to be compact and cost-effective as solid-state laser hosts and nonlinear frequency conversion media [1-4]. It is free from crucible pollution and can rapidly grow crystal fibers of different scales. However, the quality of crystal fiber is affected by the shape control of molten zone during the fiber growth. In general, the shape of molten-zone is determined by a variety of interface shapes. In theory, a symmetrical interface shape of floating zone can be obtained under the conditions of complete axial symmetry in laser heating and gravity field reversed to the growth direction. However, in the real case, in addition to the limitations of static and dynamic Bond number, the shape of molten-zone is very relevant to space symmetry of growth axis with the position of laser heating and gravity field during fiber growth. Crystal growth frame of LHPG can usually be seen as static and symmetrical in the molten zone under ideal conditions. There are many related research [5-7]. Its symmetrical shape of the molten zone is mainly affected by gravity and surface tension under the allowed power range [8]. However, the actual condition to maintain the full symmetry of space is difficult. The reason is that the influences of molten zone slightly deviate from the symmetric space and the asymmetric laser heating ring projected into the molten zone caused by seed is inconsistent with the source rod position when we manually calibrate the crystal growth system. These influences will further lead to the flow field and temperature field with asymmetry in the molten zone so that the molten zone showing instability thereby affecting the crystal quality.

For growing single-crystal fiber using LHPG method, there were only few three-dimensional numerical models [9-11]. Here the modified model of three-dimensional thermo-capillary floating zone is a calculating system of physical grid through a non-orthogonal body-fitting grid transforming and uses the control-volume finite-difference method for simulation.

In this paper, we will select a material of slightly doped Cr:YAG to discuss the growth influences caused by laser heating and gravity field slight deviation from symmetry of growth axis through the LHPG experiments and three-dimensional simulation of micro-floating zone under different size of source rods._

*Corresponding author. Tel.: +886-8-7799821 ext 6506; mobile: +886 -937-388-198.

E-mail address: x00008415@meiho.edu.tw (P.- Y. Chen)

2. Experimental Approach

The source rods were 0.5 mol.% doped Cr:YAG that were <111> in crystal orientation and 500×500 μm^2 in cross section. A 10.6-μm laser system (Synrad Firest V40, 40 W full power) with an attenuator to adjust the laser power was the heat source to enter the growth chamber. The power fluctuation can be improved from ±3% to < ±0.2% using a feedback control. Inside the chamber, the incident Gaussian laser beam was transformed into a ring-shaped semi-Gaussian beam by a reflaxicon. After the 45 degree planar mirror, the parabolidal mirror focuses the beam on the top end of the source rod as shown in Fig. 1. The oxygen-free copper paraboloidal mirror with a 25 mm focus length was fabricated by the diamond-turning technology. The use of a parabolic rather than a spherical annulus eliminates spherical aberration. The top end was heated and melted by a CO_2 laser with a donut shaped beam and a spot size of about 25 μm. The pulling and feeding mechanisms are outside the chamber, and consist of computer-controlled linear stage driven by stepping motor with gearbox to reduce vibration. After diameter-reduction steps on the LHPG system, the crystal fibers with diameters of less than 500 μm were obtained. Then, the as-grown fiber was used as the source rod to draw the fiber again through the same LHPG system.

3. Mathematical Formulation

Owing to the heating method of LHPG is based on the CO_2 laser beam through a series of optical system frame, and the beam final projection to 39 degrees to focus on the center of growth chamber. Therefore, we modified Lan's three-dimensional thermocapillary floating numerical mode in laser heating and diameter reduction type. In the x-y plane, the angle of inclination to provide gravity field α = 0 ~ 3 degrees and the heating ring plane tilting angle θ = 0 ~ 3 degrees range as asymmetrical perturbation of space for study.The laser intensity profile on the miniature MZ is approximated as an asymmetrical Gaussian distribution,

$$I_a = A_q \exp\left[-\alpha \left(r/\gamma\right)_a^2\right]$$

where A_q and γ_a a are the amplitude and width $\left(1/e^2\right)$ of the Gaussian distribution at z = 0, respectively, and α_a is the beam-shape factor[JAC,JJAP].The physical properties of YAG material and other related input parameters are shown in Table 1 [12] and Table 2. The dimensionless variables are defined by scaling length with the feed rod diameter D_f, velocity with α_m/D_f ; pressure with $\rho_m\alpha_m^2$ m=D_f^2, and temperature with the melting point T_m, where α_m is the thermal diffusivity and ρ_m the melt density. The steady-state governing equations describing the convection and heat transport in the melt are required as follows:

$$\nabla \cdot \vec{v} = 0$$
$$\vec{v} \cdot \nabla \vec{v} = -\nabla P + \mathrm{Pr}\nabla^2 \vec{v} - \mathrm{Pr}\, Ra_T \left(T - 1\right)\vec{e}_g$$
$$\vec{v} \cdot \nabla T = \nabla^2 T$$

(4)

where $\vec{v}$, P and T are the dimensionless velocity, pressure, and temperature, respectively. Also, $\mathrm{pr} = \nu_m/\alpha_m$ is the Prandtl number, where ν_m is the kinematic viscosity. The gravity direction $\vec{e}_g$ is the unit vector of gravity, which can be aligned $\left(\alpha=0^0\right)$ with or tilted $\left(\alpha=3^0\right)$ and the angle θ between heating ring plane and the horizontal plane can be adjusted from $\left(\theta=0^0\right)$ to $\left(\theta=3^0\right)$ (from the growth axis on the x-y plane, as shown in Fig. 1. Furthermore, Tm also serves as a reference temperature. The associated dimensionless number in the source term of Eq. (2) is the thermal Rayleigh number, defined as follows:

$$Ra_T = \beta_T g T_m D^3 / \nu_m \alpha_m ,$$

where β_T is the thermal expansion coefficients and g the gravitational acceleration. In the crystal (c) and the feed rod (f) only heat transfer needs to be considered:

$$v_i \vec{e}_x \nabla T = \nabla \cdot k_i \nabla T,\ i = (c, f)$$

where *r* is $k_i = \alpha_i(T)/\alpha_m$ the dimensionless thermal diffusivity of feed and crystal; α_i is the thermal diffusivity of the feed rod $(i = f)$ or the crystal $(i = c)$. Also, $\vec{e}_x$ is the unit vectors in the axial direction. In addition, most of the oxide crystals are often quite transparent to infrared. Therefore, internal radiation cannot be ignored. We have chosen the simplest model, i.e., the no-slip Rosseland diffusion model used by Vizman et al., for the crystal. Because the feed rod is usually prepared by sintering, the optical distance is small so that opacity is assumed; the melt is assumed to be opaque as well. One may consider a better model for the internal radiation, but it requires more computational effort, which is not the major interest of this study. Nevertheless, based on the same computer code, we can add a more sophisticated model for radiation if necessary.

The no-slip condition is used for the velocity at solid boundaries. At the free surface, the shear stress balance is imposed:

$$\vec{\tau} : \vec{n}\vec{s} = Ma(\partial / T\partial)$$

where $\vec{\tau} : \vec{n}\vec{s}$ is the shear stress at the *n*-*s* plane of the free surface; $\vec{n}$ and $\vec{s}$ are the unit normal and tangential vectors at the free surface, respectively. Also, Ma is the Marangoni number, which is defined as:

$$Ma = |\partial\gamma / \partial T| T_m D_f / \rho_m \nu_m \alpha$$

where $\partial\gamma/\partial T$ is the surface-tension-temperature coefficient of the melt. Two tangential directions need to be considered for the stress balance. In addition, the kinematic condition $(\vec{n} \cdot \vec{v} = 0)$ at the free surface and the normal stress balance (the Young–Laplace equation) are also satisfied, i.e.,

$$\vec{\tau} : \vec{n}\vec{n} = (2H) B_0 + \lambda_0$$

where 2*H* is the mean curvature, $B_0 = \gamma/(\rho_m g D_f^2)$ is the static Bond number; g is the surface tension of the melt. The detailed way for calculating the mean curvature can be found elsewhere. Also, λ_0 is a reference head that needs to be determined to satisfy the growth angle constraint for the steady growth or the global mass conservation for stationary melting. For the steady growth, the growth angle constraint needs to be satisfied at the melt/gas/crystal tri-junction, i.e.,

$$\vec{n}_m \cdot \vec{n}_c = \cos\phi_0$$

where $\vec{n}_m$ and $\vec{n}_c$ are the unit vectors at the melt and crystal surfaces, respectively, at the trijunction line ϕ_0 is the growth angle for the growing crystal having a constant local radius. However, the static head λ_0 is used to satisfy the global mass conservation, $A_c U_c = A_f U_f$.

The thermal boundary conditions at the growth and feeding fronts are set by the heat flux balances:

$$Q|_m - Q|_i + \gamma_c (v_i \vec{e}_x) St \cdot \vec{n} = 0,\ i = (c, f)$$

where $\vec{n}$ is the unit normal vector at the feeding or growth interface pointing to the melt. $Q|_m$, $Q|_c$, and $Q|_f$ are the dimensionless total heat fluxes at the melt, the crystal, and the feeding sides, respectively. Also, γ_c is the density ratio of the crystal to the melt. The Stefan number $St = \Delta H / Cp_m T_m$ scales the heat of fusion ΔH released during solidification to the sensible heat in the melt; Cp_m is the specific heat of the melt. The heat transfer between the sample surface and the surrounding is similar to that in the 2D case described before.

The above governing equations and their associated boundary conditions can only be solved numerically. We have developed an efficient finite volume method (FVM) scheme using the primitive variable formulation and multigrid acceleration for the free and moving boundary problems. In the present study, YAG, steady-state results are always obtained. Two levels of grids are used. The

overall iteration scheme for getting a steady-state solution is straightforward. Temperature and velocity calculations are placed in the inner iterations. After having a number of inner iterations, we find the interface shape by locating the melting point isotherm, which also provides the position for the upper and lower tri-junction rims. Then, the meniscus is calculated based on the normal stress balance, in which there is an outer iteration loop for moving the local radii and getting the reference pressure to satisfy the growth angle or constant mass constraint and the overall mass conservation. The iterations continue until all variables converge. Detailed description of the numerical method can be found elsewhere.

4. Results and Discussion

The surface tension and gravity maintain the stable conditions of the floating zone in static state. But as the molten zone occurs thermocapillary flow due to laser heating, the internal flow type will affect the stability of the molten zone. In addition to the former two parameters, visual stable and static condition of molten zone was constructed under steady state of the source rod feeding into the molten and pulling the growing crystal fiber. The complete axial symmetry of LHPG molten zone in laser heating and gravity filed were destroyed by horizontal error of the optical table, source rod with seed offset and tilt from symmetry of growth axis. Owing to double eddy flow field of the floating zone controlled mainly by the thermocapillary flow, it will induce the tilting double vorticity. And even eventually lead to flow field vibration, causing the unstable molten zone. Fig. 2 shows the captured images of the molten zone in the experiment. We adjust the height of optical table feet to obtain tilting desktop with 1.5-degree. At this point the laser heating ring remains axial symmetry. In 0.5 reduction ratio with 500-μm-diameter source rod as the base we compare molten zone offset caused by gravity filed offset to same reduction ratio with 300-μm-diameter source rod and 0.25 reduction ratio with same diameter source rod. Basically, the molten zone can maintain symmetrical type, which is due to the gravity effect to formed micro-floating zone, its scale is far smaller than the surface tension so the static Bond number become very small. This makes the possibility of growing crystal fiber with diameter below 500 μm using the LHPG method in horizontal plane. Owing to the larger tilt angle and asymmetry of the laser heating ring need to adjust the optical path with time-consuming, we added to diameter reduction and asymmetric heating conditions to modify Lan's three-dimensional thermocapillary floating numerical mode, and then analyzed the simulation results after compared with the shape of molten zone in the experiment. Fig. 3 takes 0.5 reduction ratio with 500-μm-diameter source rod in (a) all deviation 3 degrees, (b) no deviation, (c) laser heating deviation 3 degrees, (d) gravity field deviation 3 degrees, to obtained the perspective of surface temperature field of the molten zone. Basically the temperature field in (b) consist with our two-dimensional simulation results [7, 13], (a) and (c) show asymmetric temperature field caused by laser heating deviation. In order to enhance the degree of simulation and physical credibility, we take real molten zone of the experiment as the background for contrast with the shape of molten zone in the simulation. Essentially more than 90 percent similarity, it is only in the vicinity of crystal fiber necking position quite different, but overall the molten zone can generally match as shown in Fig. 4. The temperature field and flow field distribution in Fig. 4 consist with our two-dimensional simulation results [7, 13]. In order to investigate the real reasons causing the molten zone offset, Fig. 5 shows the simulation molten zone with two different power (difference in length of the molten zone) and the perturbation mechanism of solid-liquid and gas-liquid interface shape: (a) all deviation 3 degrees, (b) no deviation, (c) laser heating deviation 3 degrees, (d) gravity field deviation 3 degrees. We found only on the solid-liquid interface of crystal fiber necking location has a very small difference. The shape of molten zone has remained basically the same. Fig. 5 (b) and (c) show influences of the molten zone less obvious when the diameter reduction and source rod scale were reduced.

4. Conclusions

The modified model of three-dimensional thermo-capillary floating zone was established. It is a calculating system of physical grid through a non-orthogonal body-fitting grid transforming and uses the control-volume finite-difference method for simulation. The shape of the molten zone (especially the solid-liquid interface) by the asymmetrical heating effect is much larger than the

result of gravity field in the simulation results of tilting 3 degrees when the source rod diameter is below 500 μm. And the influence will decrease rapidly with the source rod scale and diameter reduction ratio reducing. Finally, the results can be further obtained trend charts of thermal distribution and flow field in molten zone to improve the quality of crystal fiber. At the same time the feasibility of growing crystal fiber using the LHPG method in horizontal plane could also be further investigated under suitable scale of molten zone.

Acknowledgment

This work was supported in part by National Science Council, Taiwan, ROC, under contracts NSC-96-2221-E-019-021.

References

[1] M. M. Fejer, J. L. Nightingale, G. A. Magel, R. L. Byer, Review of Scientific Instruments 55 (1984) 1791.

[2] M. J. F. Digonnet, C. J. Gaeta, H. J. Shaw, IEEE Journal of Lightwave Technology LT-4 (1986) 454.

[3] C. Y. Lo, P. L. Huang, T. S. Chou, L. M. Lee, T. Y. Chang, S. L. Huang, L. Lin, H. Y. Lin, F. C. Ho, Japanese Journal of Applied Physics 41 (2002) L1228.

[4] S. Sudo, A. Cordova-Plaza, R. L. Byer, H. J. Shaw, Optics Letters 12 (1987) 938.

[5] J. C. Chen, C. Hu, Journal of Crystal Growth 149 (1995) 87.

[6] J. C. Chen, C. Y. Lo, K. Y. Huang, F. J. kao, S. Y. Tu, S. L. Huang, Journal of Crystal Growth 274 (2005) 522.

[7] P. Y. Chen, C. L. Chang, K. Y. Huang, C. W. Lan, W. H. Cheng, S. L. Huang, Japanese Journal of Applied Physics 48 (2009) 115504

[8] G. Li, Z. Liu, Y. Lin, J. Synth. Cryst. 22 (1993) 32.

[9] C. W. Lan, B. C. Yeh, Journal of Crystal Growth 262 (2004) 59.

[10] C. W. Lan, J. H. Chian, Journal of Crystal Growth 230 (2001) 172.

[11] C. W. Lan, Journal of Crystal Growth 247 (2003) 597.

[12] C. W. Lan, C. Y. Tu, Journal of Crystal Growth 223 (2001) 523.

[13] P. Y. Chen, C. L. Chang, K. Y. Huang, C. W. Lan, W. H. Cheng, S. L. Huang, Journal of Applied Crystallography 42 (2009) 553.

Table(s)

Table1

Symbols	Values	Units	Descriptions
		Yttrium aluminum garnet; YAG	
ρ_s	3.685	$g \cdot cm^{-3}$	Density of solid
ρ_m	4.3	$g \cdot cm^{-3}$	Density of melt
T_m	1970.0	°C	Melting point
ΔH	455.5	$J \cdot g^{-1}$	Melt/solid latent heat
k_s	0.1	$W \cdot cm^{-1} \cdot °C^{-1}$	Thermal conductivity of solid*
k_m	0.1	$W \cdot cm^{-1} \cdot °C^{-1}$	Thermal conductivity of melt*
C_{ps}	1.0	$J \cdot g^{-1} \cdot °C^{-1}$	Specific heat of solid*
C_{pm}	0.39	$J \cdot g^{-1} \cdot °C^{-1}$	Specific heat of melt*
$\partial\gamma/\partial T$	-0.035	$dyn \cdot cm^{-1} \cdot °C^{-1}$	Surface-tension-temperature coefficient*
γ	780	$dyn \cdot cm^{-1}$	Surface tension*
μ_m	0.4	$g \cdot cm^{-1}s^{-1}$	Viscosity of melt
β_m	6.5×10^{-5}	K^{-1}	Thermal expansion coefficient of melt
ε_s	0.7	—	Radiation emissivity of solid
ε_m	0.5	—	Radiation emissivity of melt
		Other input parameters	
$D_{s,c}$	See Table IV	μm	Diameters of rod and fiber
$U_{s,c}$	See Table IV	μm/s	Speeds of feed and growth
L	5	cm	Rod length
h	1.1×10^{-3}	$W \cdot cm^{-2} \cdot K^{-1}$	Heat transfer coefficient
f_m	1.00~1.88	—	Factor of equivalent melt absorption
a_m	0.5	—	Gray body factor

*at melting point

Table2

Sample index	**A**	**B**	**C**
Source rod size (μm)	500	500	300
Crystal fibre diameter (μm)	250	125	150
Feed speed (mm/min)	1	4	1
Growth speed (mm/min)	4	16	4
Reduction ratio (%)	50	25	50
Higher allowed power (W)	5.1	3.6	3.6
Lower allowed power (W)	4.1	3.1	4.4

Figure(s)

Fig. 1

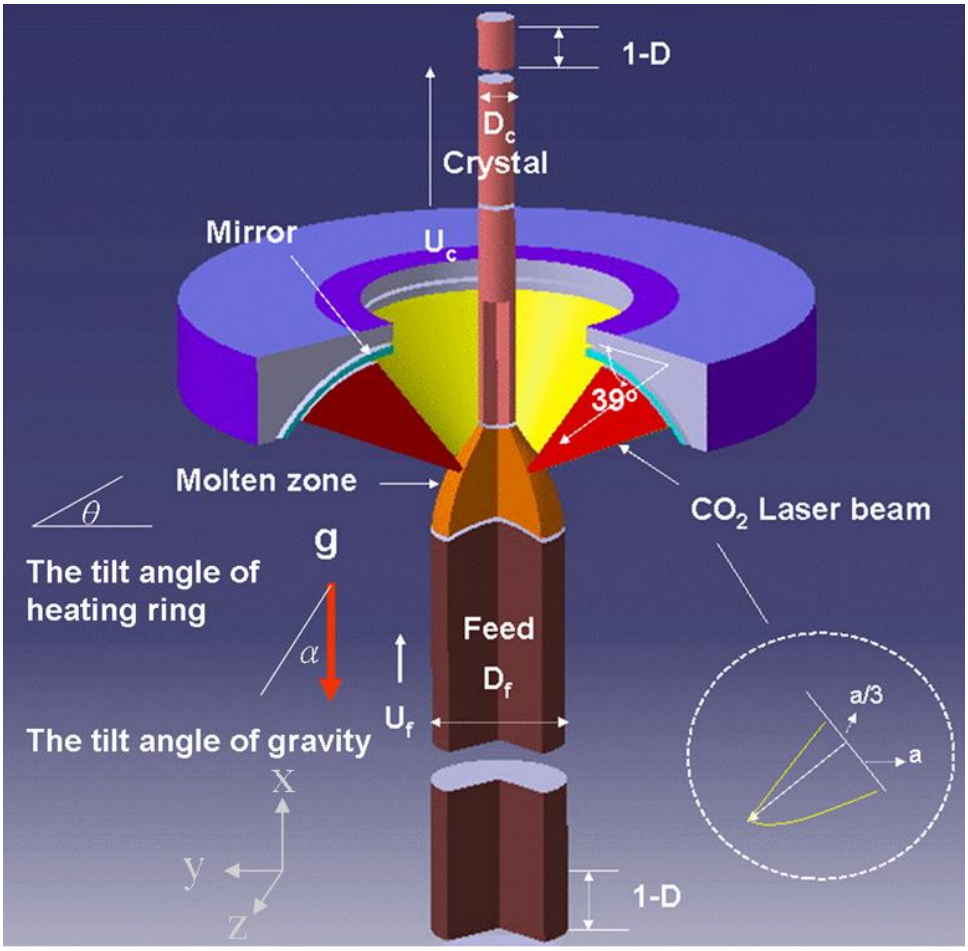

Fig. 2

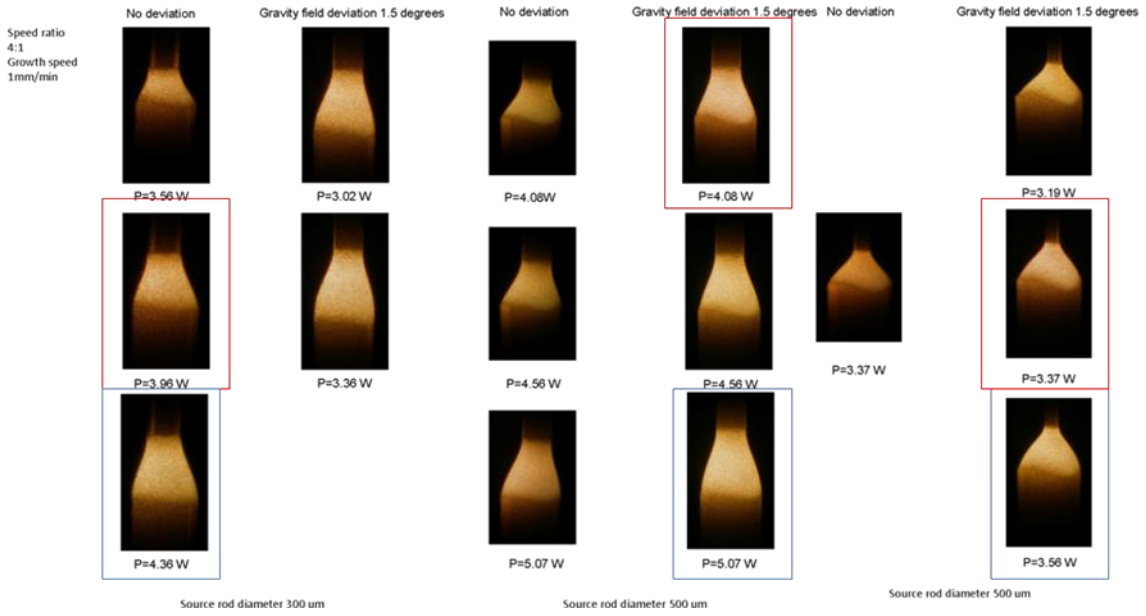
Speed ratio
4:1
Growth speed
1mm/min
No deviation
Gravity field deviation 1.5 degrees
No deviation
Gravity field deviation 1.5 degrees
No deviation
Gravity field deviation 1.5 degrees
P=3.56 W
P=3.02 W
P=4.08W
P=4.08 W
P=3.19 W
P=3.96 W
P=3.36 W
P=4.56 W
P=4.56 W
P=3.37 W
P=3.37 W
P=4.36 W
P=5.07 W
P=5.07 W
P=3.56 W
Source rod diameter 300 um
Source rod diameter 500 um
Source rod diameter 500 um

Fig. 3

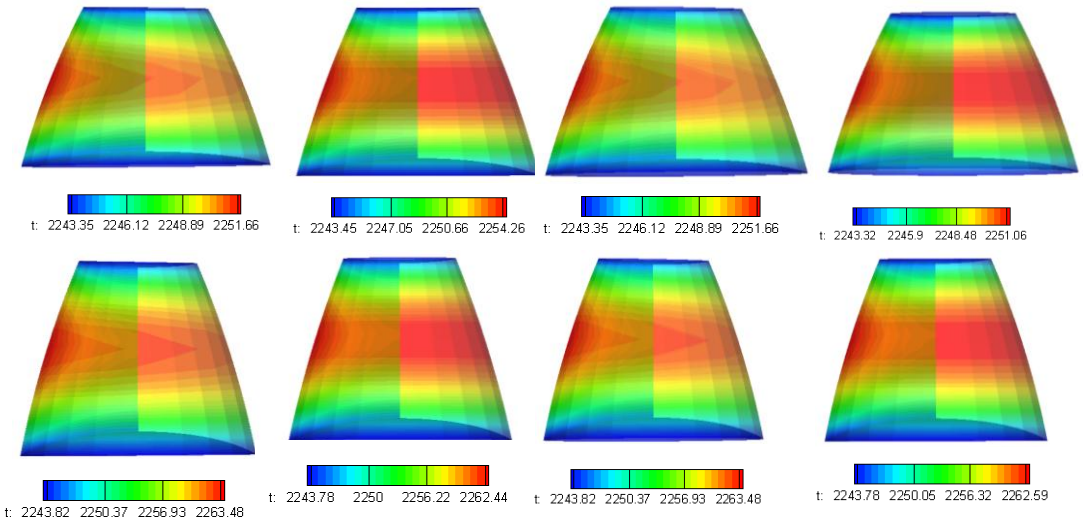
t: 2243.35 2246.12 2248.89 2251.66
t: 2243.45 2247.05 2250.66 2254.26
t: 2243.35 2246.12 2248.89 2251.66
t: 2243.32 2245.9 2248.48 2251.06
t: 2243.82 2250.37 2256.93 2263.48
t: 2243.78 2250 2256.22 2262.44
t: 2243.82 2250.37 2256.93 2263.48
t: 2243.78 2250.05 2256.32 2262.59

Fig. 4

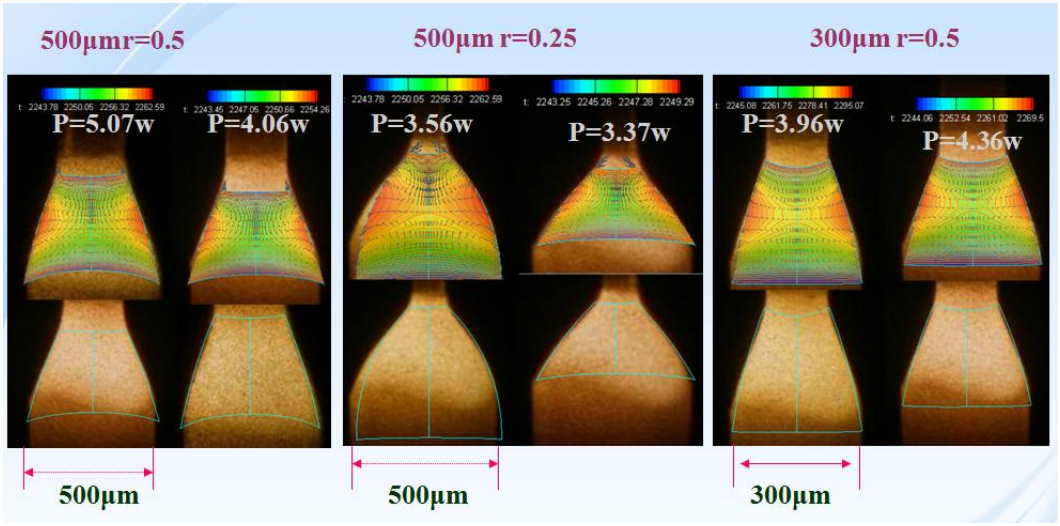
500μmr=0.5
500μm r=0.25
300μm r=0.5
P=5.07w
P=4.06w
P=3.56w
P=3.37w
P=3.96w
P=4.36w
500μm
500μm
300μm

Fig. 5

Feed rod Scale 500 μm

Higher Power

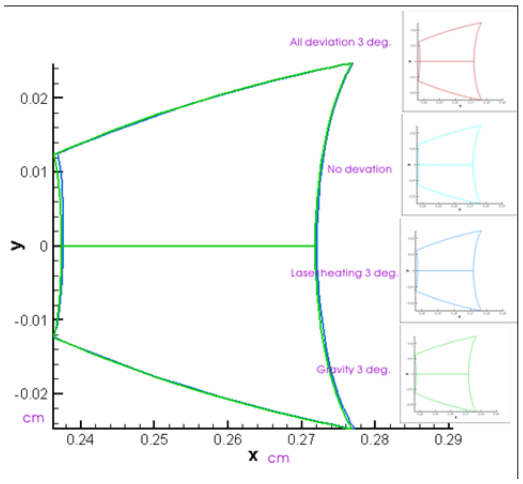

Lower Power

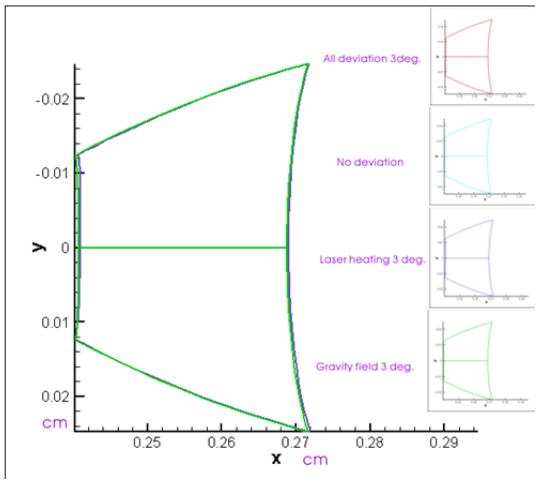

Feed rod Scale 500 μm

Higher Power

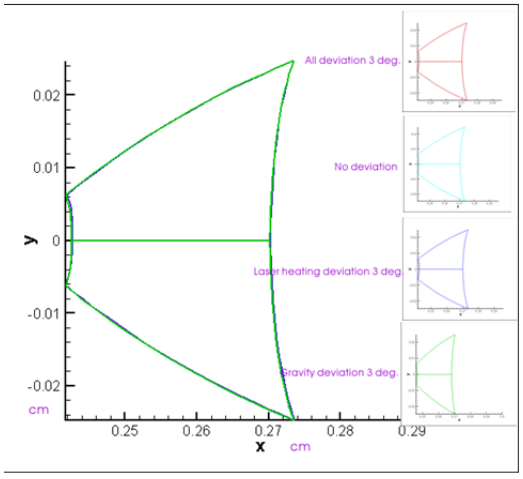

Lower Power

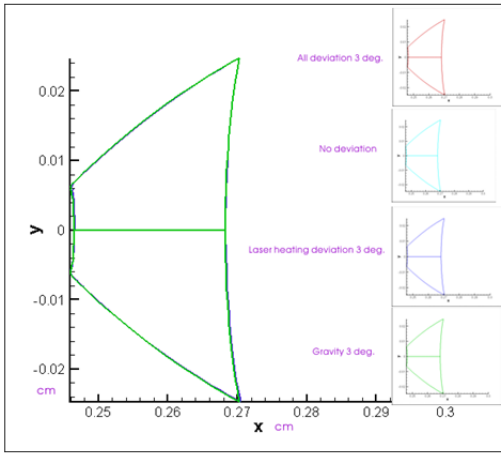

Feed rod Scale 300 μm

Higher Power

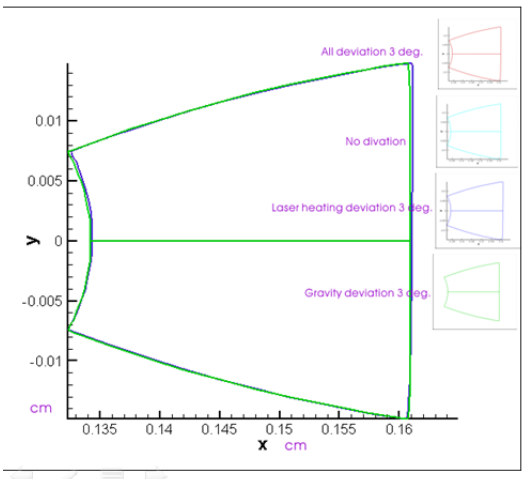

Lower Power